CHAPTER IV

Gold nanoparticles (AuNPs) functionalized electrochemically polymerized PEDOT and its application for the detection of Aflatoxin B_1 and organophosphates

This chapter focuses on the morphological, structural and electrocatalytic properties of PEDOT/GCE, AuNPs/PEDOT/GCE, BSA/anti-AFB_1/AuNPs/PEDOT/GCE and AChE/AuNPs/PEDOT/GCE electrode systems. A systematic study of electro-catalytic properties of the synthesized electrodes has been carried out by using cyclic voltammetry techniques to investigate and understand catalytic behaviour towards the redox species [$K_4(Fe(CN)_6)^{4-/3-}$].The AuNPs/PEDOT/GCE has been used to immobilize anti-AFB_1 and AChE and the sensing of the bioelectrode towards the respective analytes has been done.

4.1 Introduction

Mycotoxins are low-molecular-weight natural products produced as secondary metabolites by filamentous fungi and found to be colonizing with crops. The best known and most intensively investigated mycotoxins in the world are Aflatoxins, which are potent hepato-carcinogens [308, 309]. While more than 20 AFs have been identified, the major AFs under consideration are designated as B_1 (AFB_1), B_2, G_1 and G_2. Among them, AFB_1 is normally predominant in amount and the most toxic [310]. It is categorized as Group 1 by IARC (International Agency for Research on Cancer), which indicates there is sufficient evidence of carcinogenicity in exposed humans (IARC Monographs on the evaluation of carcinogenic risks to humans, 2002). They are difuranocoumarin derivatives produced by a polyketide pathway by many strains of Aspergillus flavus and Aspergillus parasiticus that are common contaminants in agriculture [308]. They are associated with many crops including peanuts, corn, cottonseed, Brazil nuts, pistachios, spices, copra (dried coconut) and

figs particularly in hot and humid regions of the world [309]. Several classical analytical methods have been developed for the detection and quantification of aflatoxins in agricultural products and processed food products.

Organophosphates (OPs) a derivative of phosphoric acid have been commercially used as pesticides in modern agriculture, yet their contamination still remains a severe public concern for human health and food safety due to their low persistence and high insecticidal activity [311, 312]. The toxins may enter the food chain directly or indirectly and affects the human health adversely by inhibiting the activity of acetylcholinesterase (AChE) [313] irreversibly which is a key component of cholinergic brain synapses and neuromuscular junctions. OPs can prevent nerve transmission by blocking the hydrolysis of the transmitter choline by forming a covalent bond to a serine residue in the active site of the AChE [314]. In the past various methods have been reported for the detection of aflatoxin B_1 and organophosphates and based on the principle of detection the methods can broadly be grouped into chromatographic viz. thin-layer chromatography (TLC) [315, 316] , high-performance liquid chromatography (HPLC) [317-320] and gas chromatography (GC) [321, 322], spectroscopic viz. ultraviolet (UV) [323], diode array detection (DAD), fluorescence detection (FD) or mass spectrometry (MS) [324] detectors, and immunochemical method like enzyme-linked immunosorbent assay (ELISA) [325, 326]. The chromatographic and spectroscopic methods require highly qualified expertise and extensive sample purification [327]. Moreover they require well-equipped laboratory facilities, time-consuming sample pre-treatment and also required multiple steps [327]. Although these assays could quantitatively provide an accurate evaluation of the health risk of integrated aflatoxin B_1 and OPs exposure, they are beyond the means of poor developing countries like India where the risk of illness and outbreak are greatest. Hence, simple, sensitive, selective, and portable tools are still highly desired for biomonitoring and diagnostic in order to overcome intrinsic disadvantages of either low detection specificity and sensitivity, or expensive analysis settings entailing well-trained personnel and inconvenience for field applications [328, 329].

Immunoassays based on electrochemical methods are relatively simple and easy-to-use methods for detection of AFB_1 in different food products in comparison to those chromatographic methods [330, 331]. Amperometric enzymatic

acetylcholinesterase inhibition based biosensors fabricated from different nanocomposites have been emerged as valuable tools in the field of organophosphates (OPs) detection [332-334].

Electrochemical biosensors can be a potential alternative to the classical methods due to their good selectivity, sensitivity, rapid response, and miniature size [335]. There are certain challenges during the fabrication of electrochemical enzyme based electrodes mainly (i) providing large surfaces for enzyme immobilization; (ii) preventing enzymes from leaking out of the surfaces; (iii) maintaining the enzymes' activities [336]. With an aim to minimize these problems, novel nanomaterials have been used in fabrication of electrochemical biosensors, such as nanogold [337], carbon nanomaterials [338, 339], magnetic nanoparticles, semiconductor quantum dots (QDs), silica nanoparticles and hybrid nanostructures [340-343] in order to improve the sensitivity and simplify the detection. Among them gold nanoparticle (AuNPs) based electrochemical, optical and piezoelectric detection have drawn particular interest in the bioanalytical field due to their superior physical and chemical properties such as easy fabrication, compatibility and unique catalytic activity [344, 345]. The nanoparticles modify the electrode substrate by creating nanostructured surfaces with improved electrochemical response. It also acts as a carrier for the immobilization of biomolecules like enzymes, antibodies and protein conjugates, for electrochemical signal transduction and amplification [346, 347]. However, gold nanoparticles easily tend to aggregate during the application process with the change of conditions like pH and temperature [348]. In the present thesis work AuNPs are stabilized by depositing them on a matrix of conducting polymer, Poly (3, 4-ethylene dioxythiophene) PEDOT.

PEDOT is one of the most promising conducting polymers and it has been used in biological and biomedical areas such as biosensors and bio-interface [349] as the deposition of PEDOT on electrode surface would effectively improve the electrochemical performance of the modified electrodes [350]. It can be electropolymerized from 3,4-ethylene dioxythiophene (EDOT) monomer and the oxidative polymerization of PEDOT results in positive charges on the polymer backbone, this allows for the incorporation of negatively charged doping agents, such as graphene oxide (GO) [351], AuNPs [352], polystyrene sulfonate [353], carbon nanotubes (CNT) [354] for the purpose of charge balancing. Moreover its

mechanical strength are compatible with flexible matrix, which can endow fine mechanical property for biological systems and once doped with other functional materials, the surfaces of PEDOT composites can possess many functional groups, tending to be an ideal substrate to bond with multifunctional biomolecules, such as antibody, for the fabrication of desirable biological systems [352].

In the present thesis work, a new multi-component matrix consisting of PEDOT and gold nanoparticles (Au-NPs) has been developed for the immobilization of anti aflatoxin B_1 (anti-AFB_1) antibodies and acetylcholine esterase for efficient detection of AFB_1 and methyl parathion (MP), respectively. The bioelectrode has been synthesized with a view to enhance the sensitivity towards the detection of AFB_1 and MP. Field emission Scanning Electron Microscope (FESEM) (JEOL-JSM-6390LV) to study the morphology of the synthesized nanocomposites. The surface characteristic have been studied using contact angle measurements have been made by Degree of Hydrophilicity measurement set up (Model: DSA 15B). The conformational changes in the materials have been studied using vibrational spectroscopy employing Fourier Transform Infrared (FTIR) spectroscopy. The electrochemical impedance spectroscopy (EIS) has been employed to investigate the resistance encountered in the charge transfer mechanism at the interface of the electrode and the electrolyte solution. The electro-catalytic properties and the electron transfer mechanism have been studied using cyclic voltammetry (CV). The sensitivity of the synthesized composites towards analytes has been studied and the real sample analysis of spiked and unspiked samples has been done using DPV. The real time /analysis of the spiked and unspiked samples have been carried out using differential pulse voltammetry techniques.

4.2 Morphological Analysis:

The morphology of (A) PEDOT, (B) AuNPs/PEDOT, (C) BSA/anti-AFB_1/AuNPs/PEDOT and (D) AChE/AuNP/PEDOT films has been seen using FESEM and presented in Figure 4.1. The FESEM for PEDOT shows sponge like rough structure with slightly porous nature of the surface. After deposition of the Au-NPs the porosity of the surface increases and the nanoparticles are deposited onto the surface of PEDOT. The Au-NPs are less agglomerated as the PEDOT film provides a stable surface and resists the agglomeration in between the particles. The

average size of the Au-NPs is estimated to be in the range of 230 nm to 300 nm. Figure 4.1 (C & D) clearly depict that the porosity and the surface area of the synthesized film decreases which is an indication of successful immobilization of the anti-AFB_1 and AChE on the electrode surface.

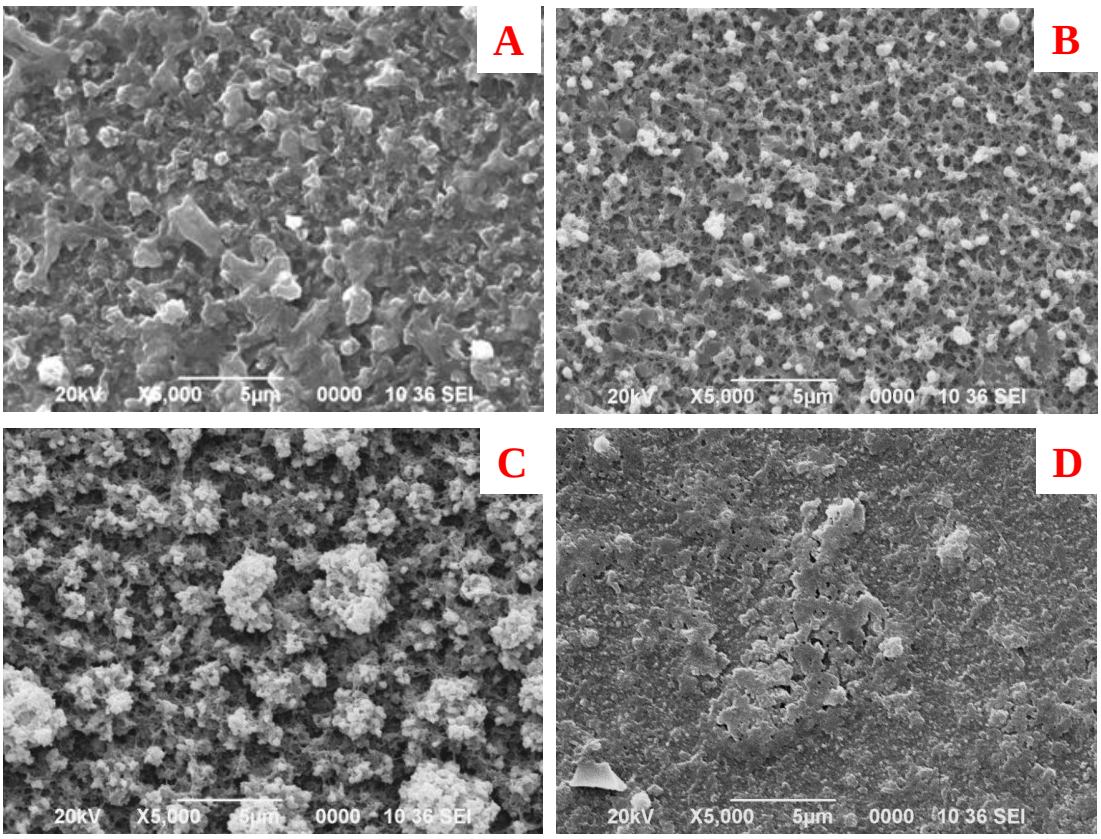

Figure 4.1: FESEM Micrograph of (A) PEDOT, (B) AuNPs/PEDOT, (C) BSA/anti-AFB1/AuNPs/PEDOT and (D) AChE/AuNPs/PEDOT films.

4.3 Contact angle Measurement:

Figure 4.2 (A & B) shows the contact angle measurement for PEDOT/GCE and AuNPs/PEDOT/GCE and the calculated values are 76^0 and 54^0 respectively. The contact angle of the surface before immobilization has been done to measure the degree of hydrophilicity as the surface hydrophilicity is an important factor for the immobilization of the protein [355]. The functionalization of PEDOT matrix with Au-NPs results in decrease in contact angle making the film more hydrophilic. The antibody immobilization requires a hydrophilic surface as the protein loses its β-sheets configuration at hydrophobic surfaces, confirming a general trend in structural

change. The hydrophobicity of surface contributes to unwanted interactions between the proteins and the matrix. This could generate a problem with unspecific binding [355].

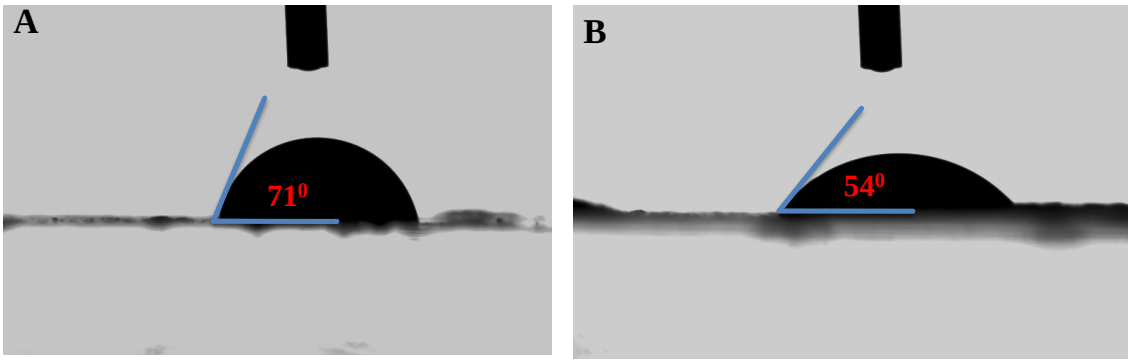

Figure 4.2: Contact angle measurements of (A) PEDOT and (B) AuNPs/PEDOT film.

4.4 FTIR spectroscopy:

The FTIR spectra of the synthesized PEDOT, AuNPs/PEDOT/GCE, BSA/anti-AFB_1/ AuNPs/PEDOT/GCE and AChE/AuNPs/PEDOT/GCE are shown in Figure 4.3. The vibrational bands observed around 1345 cm^{-1} and 1524 cm^{-1} correspond to the C–C or C=C stretching of the thiophene ring. The vibration bands at 1140 $cm^{-1}$and 1051 cm^{-1} are due to the C–O–C bond stretching in the ethylenedioxy group. The absorption bands at 843cm^{-1} and 672 cm^{-1} are assigned to thiophene C–S bond stretching [356]. The vibrational bands at 3418 cm^{-1} are attributed to the O–H stretching vibrations, respectively. The vibration bands observed in the wavenumber range of 2800–3000 cm^{-1} are assigned to the C–H stretching mode [357]. The absorption peak at 1720 cm^{-1} is usually associated with the doped state of PEDOT [356]. For BSA/anti-AFB_1/AuNPs/PEDOT/GCE curve in Figure 4.3, the amide I band at 1654 cm^{-1}, amide II band at 1564 and 1252 cm^{-1} demonstrate immobilization of antibodies [358] onto Au-NPs modified PEDOT surface.

Similarly the immobilization of AChE enzyme is confirmed by two vibration peaks between at 1684 cm^{-1} and 1560 cm^{-1} which concludes the retain of native nature of the enzyme in the bioelectrode AChE/AuNPs/PEDOT/GCE [359].

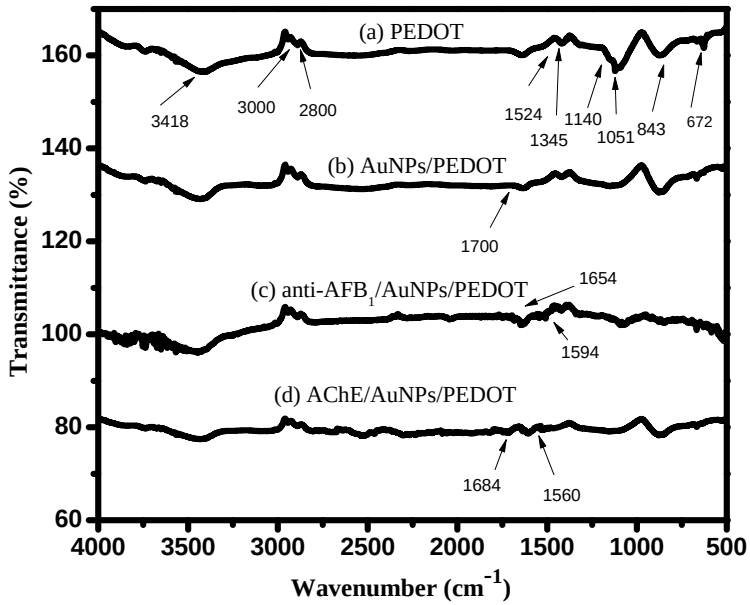

Figure 4.3: FTIR Spectra of PEDOT, AuNPs/PEDOT and BSA/anti-AFB_1/AuNPs/PEDOT and AChE/AuNPs/PEDOT films.

4.5. Electrochemical Impedance Spectroscopy:

Electrochemical Impedance Spectroscopy study was performed on bare GCE, PEDOT/GCE, AuNPs/PEDOT/GCE, BSA/anti-AFB_1/PEDOT/GCE and AChE/AuNPs/PEDOT/GCE to investigate the resistance occurring in the charge transfer mechanism within the interface of the electrode and the electrolyte solution. The experiment has been carried out in an electrochemical cell comprising of three electrodes and a standard Fe $[(CN)_6]^{3-/4-}$ solution as the redox probe.

The equivalent circuit for the electrode and electrolyte combination within the Randles cell is shown in Scheme 4.1.

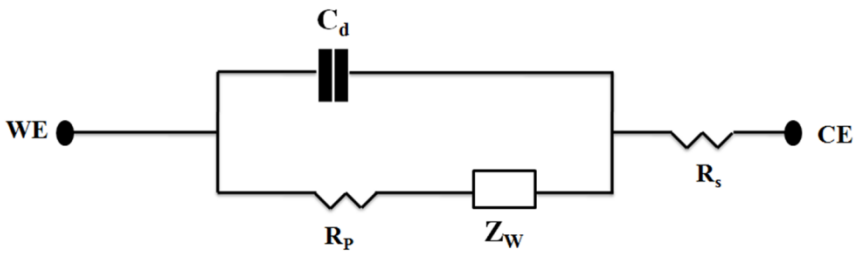

Scheme 4.1: The equivalent circuit representing the Randles Cell.

The electrochemical complex matrix (Z) can be represented as the sum of the real (Z') and imaginary ($-Z''$) components [$Z = Z' + j\ (-Z'')$, where $j = \sqrt{-1}$] with Φ (the phase angle) = $\tan^{-1}$ [$Z''\ (\omega)/Z'\ (\omega)$] [360]. Both Nyquist and Bode Plots were obtained at different frequencies and used to determine the relative change in the polarization resistance R_P at zero potential. The equation of the parallel RC circuit is as follows:

$$Z(\omega) = Z' + Z'' = \frac{R_s + R_p}{(1 + j\omega C_{dl})} \tag{4.1}$$

$$Z' = \frac{R_s + R_p}{1 + \omega^2 R_p^2 C_{dl}^2} \qquad \text{And} \qquad -Z'' = \frac{\omega R_p^2 C_{dl}}{1 + \omega^2 R_p^2 C_{dl}^2} \tag{4.2}$$

Where, R_s is the ohmic resistance of the solution between working electrode and the counter electrode and R_p is the polarization resistance. At zero potential R_p can be described as electron transfer resistance R_{et} and C_{dl} is the double layer capacitance arising from the accumulations of charges in the electrode-electrolyte interface. The relationship between the frequency associated with maximum value of Z'' (ω) and charge transfer resistance R_{et} is as follow:

$$R_{et} C_{dl} = \frac{1}{2\pi f_{max}} \tag{4.3}$$

Figure 4.4 (A) & (B) shows the Nyquist plot ($-Z''$ vs. Z') at different frequencies and the corresponding Bode Plot [Z vs. Log (ω)]. The calculated values of R_{et} and R_s are tabulated in Table. 4.1. The value of R_{et} for bare GCE is 350 Ω which decrease to 113 Ω after deposition of PEDOT on GCE. It may be due to the semi conducting nature of PEDOT which allows enhanced transfer of electrode between electrode and the medium [361]. After functionalization of PEDOT/GCE with Au-NPs the R_{et} value decreases dramatically to 67 Ω which is an evidence of more conductive nature of the medium implying that the AuNPs are acting as good conducting materials and hence the electron transfer between the redox probe and the electrode is enhanced [362]. The electron transfer resistance (R_{et}) of BSA/anti-AFB_1/AuNPs/PEDOT/GCE and AChE/ AuNPs/PEDOT/GCE is much larger around 753 Ω and 990 Ω, respectively manifesting that the antibody/enzyme film has been formed and obstructs electron transfer of the redox probe. Due to the non-conducting nature of protein, the electron-transfer of $[Fe(CN)_6]^{3-/4-}$ is blocked and the interfacial resistance increases greatly [360]. Similar information is obtained from the Bode

plot, phase angle shift plot and the double layer capacitance (C_{dl}) can be calculated using equation 4.4:

$$\omega(\Phi_{max}) = \sqrt{1/C_{dl}R_p \times (1 + \frac{R_p}{R_s})} \quad (4.4)$$

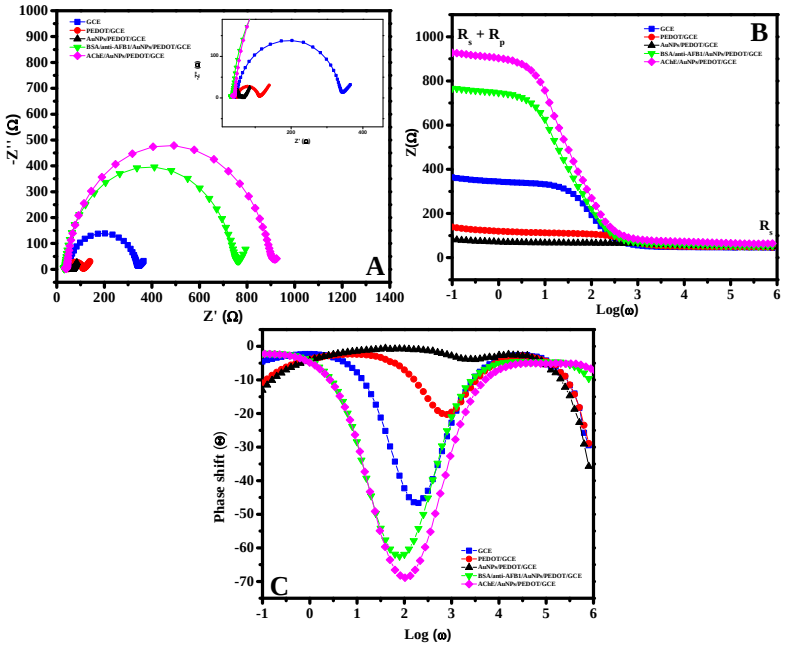

Figure 4.4 : EIS pattern of all modified electrodes (A) Nyquist Plot (Z′ vs. -Z′′), (B) Bode plot (Z vs. Log ω) and (C) Phase shifts in 100mM PBS and 5mM $[Fe(CN)_6]^{3-/4-}$.

Table 4.1: The calculated value of R_{et}, C_{dl} and Φ for the modified electrodes.

Electrodes	**R_{et}**	**C_{dl}**	**Φ**
GCE	350	7.1×10^{-6}	-46.30
PEDOT/GCE	113	2.7×10^{-6}	-20.30
AuNPs/PEDOT/GCE	67	7.4×10^{-7}	-4.38
BSA/anti-AFB_1/ AuNPs/PEDOT/GCE	762	1.5×10^{-5}	-62.59
AChE/ AuNPs/PEDOT/GCE	990	4.4×10^{-5}	-68.86

The value of C_{dl} for bare GCE, PEDOT/GCE, AuNPs/PEDOT/GCE, BSA/anti-AFB_1/ AuNPs/PEDOT/GCE and AChE/AuNPs/PEDOT/GCE has been calculated (Table 4.1). The C_{dl} value is maximum for BSA/anti-AFB_1/AuNPs/PEDOT/GCE and AChE/AuNPs/PEDOT/GCE implying that the

accumulation of charges in the electrode electrolyte interface is more in the bioelectrodes which may not allow efficient transfer of electron between the electrode and the medium. This is in accordance with the results obtained from Nyquist Plot and the cyclic voltammetry analysis. At the intermediate frequencies the phase angle value also approaches 90^0 in case of BSA/anti-AFB_1/AuNPs/PEDOT/GCE and AChE/AuNPs/PEDOT/GCE which shows the more capacitive behaviour of the electrode [231].

4.6 Cyclic Voltammetry Studies:

4.6.1 Electrocatalytic behaviour of modified electrodes towards redox species:

Cyclic voltammetry has been done to study the electrocatalytic behaviour of all the modified electrodes towards the transfer of redox species $[Fe(CN)_6]^{3-/4-}$. Figure 4.5 shows the variation of (A) cyclic voltammograms (CVs) obtained for Bare GCE, PEDOT/GCE, AuNPs/PEDOT/GCE electrodes in 100mM PBS (pH 7.4) (B) cyclic voltammograms (CVs) obtained for (a) Bare GCE, (b) PEDOT/GCE, (c) AuNPs/PEDOT/GCE and (C) CVs obtained for (a) BSA/anti-AFB_1/AuNPs/PEDOT/GCE and (b) AChE/AuNPs/PEDOT/GCE electrodes in 100mM PBS (pH 7.4) containing 5mM $[Fe(CN)_6]^{3-/4-}$ at a scan rate of 5mV/s. In PBS there are no prominent peaks of PEDOT while the reduction peak of AuNPs at 0.45 V is visible. In presence of redox species the bare GCE shows two prominent peaks with ΔE_p (E_{pa} - E_{pc}) value of 287 mV which decreases to 214 mV for GCE modified with PEDOT.

The I_{pa} and I_{pc} for PEDOT/GCE are 61.02 μA and -60.23 μA respectively which are larger than bare GCE. This can be due to the fairly conducting nature of PEDOT [363] which provides better transfer of electron within the matrix in comparison to bare GCE. After the modification of PEDOT/GCE with AuNPs, the value I_{pa} and I_{pc} increases to 94.17 μA and 91.61 μA ($I_{pa}/I_{pc} \sim 1$) respectively (curve c). AuNPs not only have excellent adsorption abilities to increase the effective area of the electrode surface in response to $[Fe(CN)_6]^{3-/4-}$, but also have high aspect ratio and good enhancement effect to $[Fe(CN)_6]^{3-/4-}$ [364], leading to the increased current and decrease ΔE_p (176 mV) in the case of AuNPs/PEDOT/GCE in comparison to

bare GCE and PEDOT/GCE. The reduced value of ΔE_p is an indication of increase in the number of electrons involved in a reaction (n α $1/\Delta E_p$) [365]. After immobilization with AChE and anti-AFB_1 the peak current (I_{pa} and I_{pc}) decreases and also the peak to peak separation increases which indicates slow transfer of redox species between the bioelectrode and the redox electrolyte.

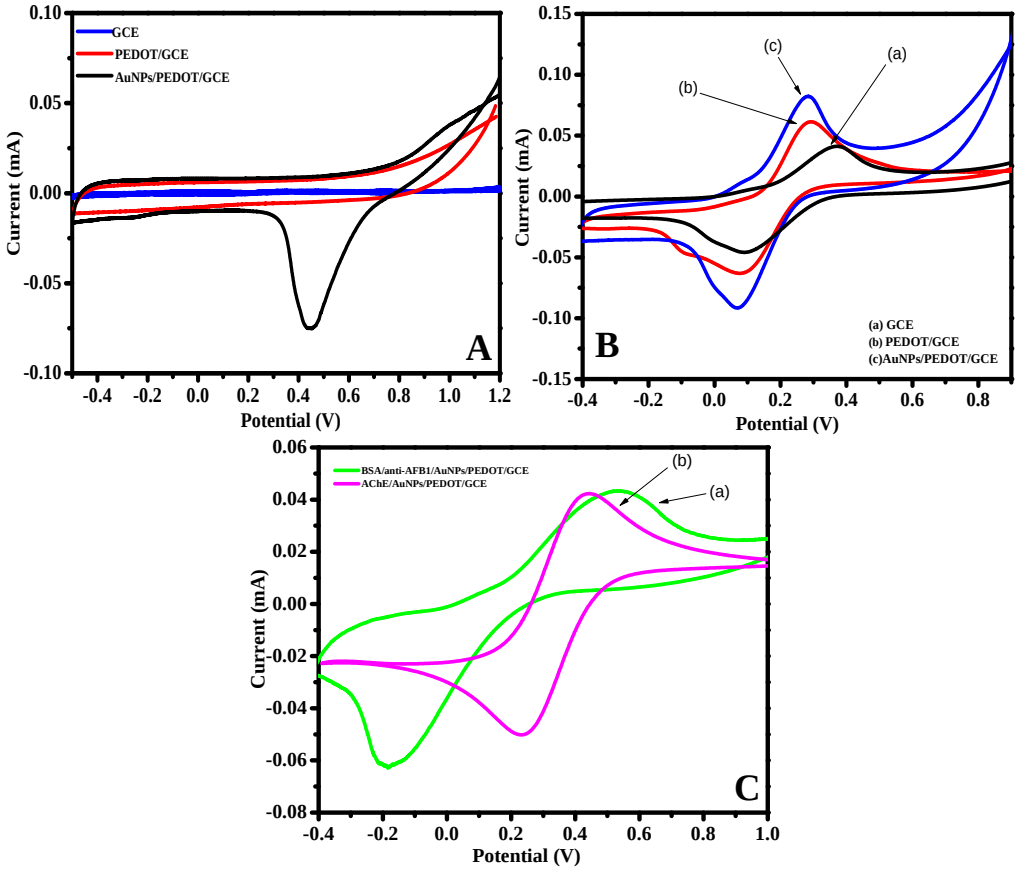

Figure 4.5: The Cyclic Voltammogram of (A) Bare GCE, PEDOT/GCE and AChE/AuNPs/PEDOT/GCE in 100mM PBS and Cyclic Voltammogram of (B) (a) Bare GCE, (b) PEDOT/GCE and (c) AChE/AuNPs/PEDOT/GCE and (C) (a) BSA/Anti-AFB_1/AuNPs/PEDOT/GCE and (b) AChE/AuNPs/PEDOT/GCE in 100mM PBS and 5mM $[Fe(CN)_6]^{3-/4-}$ at 5 mV/s vs. Ag/AgCl.

Table 4.2: The values of peak current (I_{pa} and I_{pc}) and peak to peak ΔE_p

Electrodes	**I_{pa}**	**I_{pc} (-ve)**	**ΔE_p (E_{pa}-E_{pc}) (mV)**
GCE	42.12 μA	44.81μA	287 mV
PEDOT/GCE	61.02	60.23 μA	214 mV
AuNPs/PEDOT/GCE	94.17μA	89.61 μA	176 mV
BSA/anti-AFB1/AuNPs/PEDOT/GCE	44.47μA	62.17 μA	390 mV
AChE/AuNPs/PEDOT/GCE	42.47μA	50.17 μA	203 mV

4.6.2 Variation of Anodic (I_{pa}) and Cathodic Current (I_{pc}) vs. scan rate (v):

Figure 4.6 shows the variation of CV pattern for (A) PEDOT/GCE, (B) AuNPs/PEDOT/GCE, (C) BSA/Anti-AFB_1/AuNPs/PEDOT/GCE and (D) AChE/AuNPs/PEDOT/GCE at different scan rate ranging from 5 mV/s to 30 mV/s vs. Ag/AgCl. Variation of scan rate during cyclic voltammetry measurements is important as increasing scan rate causes the electrode reactions to go from faradic range of charge- transfer to that of diffusion control [366].

Figure 4.7 displayed a relative variation of the values of peak currents I_{pa} and I_{pc} current with logarithm of scan rate for all the three electrodes .With increasing scan rate the peak current increases steadily with good uniformity of the current function, $I_p/AC\upsilon^{1/2}$. According to Randles Sevcik equation [237, 238] the intensity of peak current is estimated to depend on the surface area of the working electrode and the concentration of the electro-active species. Further the diffusion coefficient is found to be dependent on the slope of peak current (I_{pa} & I_{pc}) vs. scan rate where linear response with the scan rate shows a diffusion controlled process. The linear variation of peak current with $\upsilon^{1/2}$ indicates Randles Sevcik nature with positive correlation factor of 0.98 which implies the mass transport is the means of diffusion [237, 238].

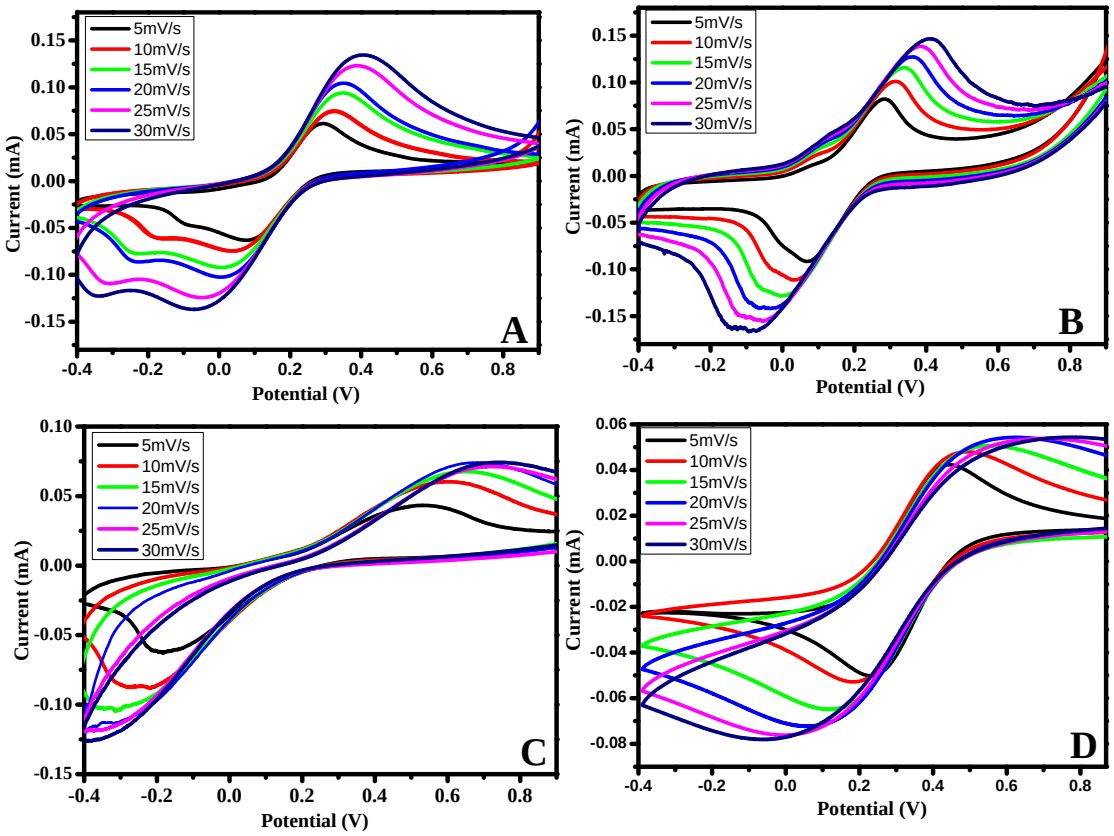

Figure 4.6: The Cyclic voltammogram of (A) PEDOT/GCE, (B) AuNPs/PEDOT/GCE, (C) BSA/anti-AFB_1/AuNPs/PEDOT/GCE and (D) AChE/AuNPs/PEDOT/GCE in 100mM PBS and 5mM $[Fe(CN)_6]^{3-/4-}$ at scan rate ranging from 5 to 30 mV/s vs. Ag/AgCl.

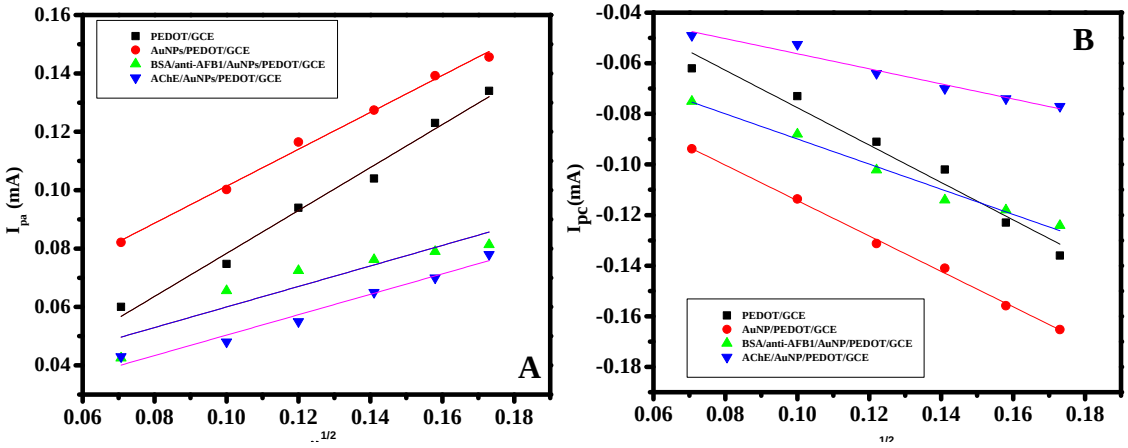

Figure 4.7: The variation of I_{pa} and I_{pc} of PEDOT/GCE, Au-NPs/PEDOT/GCE and BSA/anti-AFB_1/ AuNPs/PEDOT/GCE and AChE/AuNPs/PEDOT/GCE w.r.t square root of scan rate in V/s.

The regression equation for the linear variation of I_{pa} and I_{pc} vs. $\upsilon^{1/2}$ for AuNPs/PEDOT/GCE is as follows:

$$I_{pa}(mA) = 0.734 \times \upsilon^{\frac{1}{2}} + 0.00471;\ R^2 = 0.98 \quad 4.5$$

$$I_{pc}(mA) = -0.738 \times \upsilon^{\frac{1}{2}} + (-0.0036);\ R^2 = 0.99 \quad 4.6$$

Where 0.734 and -0.738 are slopes of I_{pa} and I_{pc} vs. $\upsilon^{1/2}$,respectively.

The slope of both anodic and cathodic peak currents (I_{pa} & I_{pc}) are smaller in bare GCE and PEDOT/GCE which increases after functionalization with Au-NPs (Table 4.3). The presence of AuNPs facilitates the redox processes within the electrode by reducing the electron transfer resistance which is in accordance to the EIS results. Further the slopes of all the modified electrodes have been calculated using Randles-Sevcik equation (equation 4.7) and the calculated values have been tabulated in Table 4.3:

$$I_p = 0.446\, nFAC\, (\frac{nF\nu\, D}{RT})^{1/2} \quad 4.7$$

The slopes of the regression equation of GCE, PEDOT/GCE and AuNPs/PEDOT/GCE have been used to calculate the electro active area. The value of electro active area increases as GCE < PEDOT/GCE < AuNPs/PEDOT/GCE and the two fold increase in the area after functionalization of PEDOT/GCE with AuNPs is attributed to the presence of high aspect ratio spherical nanoparticles over the matrix of PEDOT film.

Therefore AuNPs/PEDOT/GCE has been considered as the better electrode and taken to immobilize the enzyme and the antibody. However the linearity slope of BSA/anti-AFB_1/AuNPs/PEDOT/GCE and AChE/AuNPs/ PEDOT/GCE bioelectrode decreases. This may be attributed to the reason that after immobilization of anti-AFB_1 and AChE the peak currents decreases subsequently with increase in scan rate due to slow redox process indicating a steady state has reached and anti-AFB_1 shows an adsorptive nature at the fabricated electrode.

Table 4.3: The value of slopes of the regression equation of the linear plot of peak current vs. square root of scan rate ($v^{1/2}$).

Electrode	Anodic Slope	Cathodic Slope (-ve)
PEDOT/GCE	0.631	0.738
AuNPs/PEDOT/GCE	0.735	0.70
BSA/anti-AFB1/AuNPs/ PEDOT/GCE	0.35	0.49
AChE/AuNPs/ PEDOT/GCE	0.349	0.298

Table 4.4: The calculated values of electro active surface area.

Electrode	Electro-active area (cm^2)
GCE	0.089
PEDOT/GCE	0.163
AuNPs/PEDOT/GCE	0.215

Figure 4.8 shows the variation of peak current versus scan of the BSA/anti-AFB_1/ AuNPs/PEDOT/GCE and AChE/AuNPs/PEDOT/GCE in order to calculate the surface coverage of the anti-AFB_1 and AChE over the surface of AuNPs/PEDOT/GCE. The surface concentration of the immunosensor was calculated from the plot of current versus potential using equation $I_p = n^2F^2I^*A\upsilon/4RT$ [248]. In this equation, n is the number of electrons transferred, F is the Faraday constant, I^* is the surface concentration ($molcm^{-2}$) of the resulting immunosensor, A is the surface area of the electrode, υ is the scan rate (10 mVs^{-1}), R is the gas constant and T is the absolute temperature. The slope of the plot of current (I_p) versus scan rate (υ) gives the value of I_p/υ and hence the value of surface coverage after immobilization of antibody/enzyme can be calculated. The values of surface coverage of anti-AFB_1 and AChE in the PEDOT/GCE have also been calculated (Table 4.5). The surface coverage of the proteins have been found to be more in AuNPs modified PEDOT film as the nanoparticles helps in better immobilization of anti-AFB_1 and AChE [347].

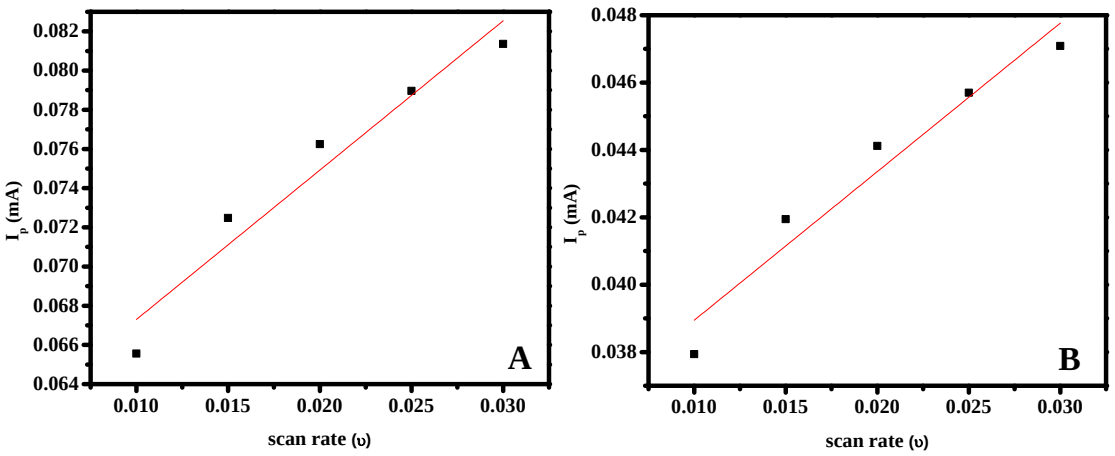

Figure 4.8: The variation of I_p of (A) BSA/anti-AFB_1/AuNPs/PEDOT/GCE and (B) AChE/AuNPs/PEDOT/GCE vs. Scan rate (V/s).

Table 4.5: The calculated values of surface concentration of anti-AFB_1 and AChE immobilized in PEDOT/GCE and AuNPs/PEDOT/GCE, respectively.

Protein	Surface concentration (I*) in PEDOT/GCE ($molcm^{-2}$)	Surface concentration (I*) in AuNPs/PEDOT/GCE ($molcm^{-2}$)
anti-AFB_1	3.4×10^{-6}	1.16×10^{-5}
AChE	5.27×10^{-8}	6.7×10^{-6}

4.6.3 Variation of Anodic (E_{pa}) and Cathodic (E_{pc}) peak potential vs. Scan rate (v):

The shifting in the position of peak potentials (E_{pa} & E_{pc}) of cyclic voltammogram of PEDOT/GCE and AuNPs/PEDOT/GCE with the logarithm of scan rate has been studied and plotted in Figure 4.9. According to Laviron's method [254] the anodic and cathodic peak potentials can be used to calculate the transfer coefficient (α) and heterogeneous electron transfer constant (k_s) according to the following relation:

$$E_{pc} = E^0 - 2.3RT\frac{log\upsilon}{\alpha nF} \quad (4.8)$$

$$E_{pa} = E^0 + 2.3RT\frac{log\upsilon}{(1-\alpha)nF} \quad (4.9)$$

$$logk_s = \alpha log(1-\alpha) + (1-\alpha)log\alpha - log\frac{Rt}{n\upsilon F} - \frac{\alpha(1-\alpha)nF\Delta E_p}{2.3RT} \quad (4.10)$$

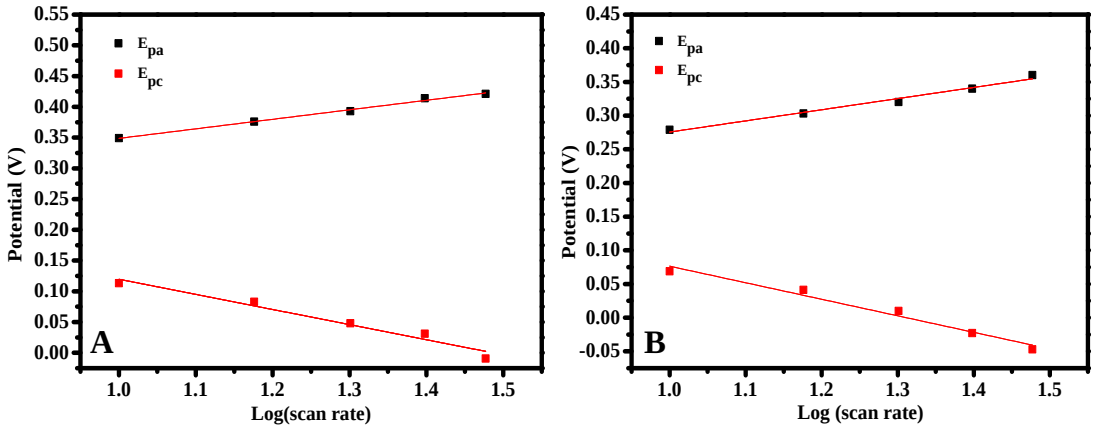

Figure 4.9: Variation of peak voltages (E_{pa} and E_{pc}) of (A) PEDOT/GCE and (B) AuNPs/PEDOT/GCE versus Log (scan rate) in 100mM PBS and 5mM $[Fe(CN)_6]^{3-/4-}$.

where α is the electron transfer coefficient, *n* is the electron transfer number, k_s is the heterogeneous electron transfer rate constant, R is the gas constant, T is the absolute temperature, and ΔE_p is the peak-to peak separation. The values of α and k_s can be estimated from the slopes of the plot of E_{pa} and E_{pc} vs. Log υ and the calculated values are tabulated in Table 4.6, respectively.

Table 4.6: The calculated values of heterogeneous rate transfer constant (k_s) and transfer coefficient (α).

Electrode	k_s (s^{-1})	α ($\alpha_a + \alpha_c$)
PEDOT/GCE	7.98×10^{-2}	0.85
AuNPs/PEDOT/GCE	1.91×10^{-1}	0.91

The comparison of k_s values indicates that the electron transfer between the medium and the electrode is faster on AuNPs/PEDOT/GCE implying enhance electron transfer which is attributed to the presence of conducting Au-NPs [347]. Therefore we can consider AuNPs/PEDOT/GCE as a suitable electrode for immobilization of antibody to achieve better performance with enhanced sensitivity.

Figure 4.10 shows the variation of ΔE_p with the $\upsilon^{1/2}$ for (i) PEDOT/GCE, (ii) AuNPs/PEDOT/GCE, (iii) BSA/anti-AFB_1/AuNPs/PEDOT/GCE and (iv) AChE/AuNPs/PEDOT/GCE. The linear increase in peak voltage with the scan rate

shows a quasi reversible mechanism which is characterized by slow kinetics of electron transfer within the electrodes [243].

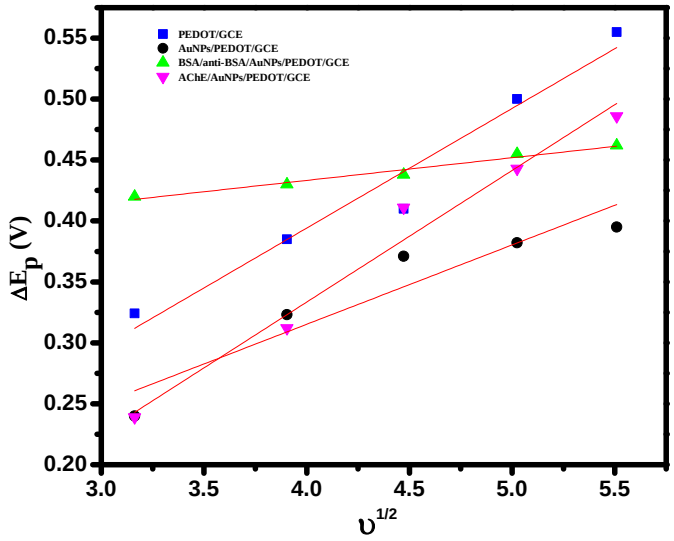

Figure 4.10: Variation of peak voltages ΔE_p (E_{pa}-E_{pc}) vs. $v^{1/2}$ of PEDOT/GCE, AuNPs/PEDOT/GCE, BSA/anti-AFB_1/AuNPs/PEDOT/GCE and AChE/AuNPs/PEDOT/GCE versus square root of scan rate.

4.7 Application of BSA/anti-AFB_1/AuNPs/PEDOT to detect AFB_1:

4.7.1 Optimization of experimental parameters:

The sensing of aflatoxin B_1 is based on monitoring the decrease in peak current as a function of concentration of aflatoxin B_1. Poor electrode stability may result in decrease in the DPV signal during the sensing of analyte. Therefore the stability of the synthesized electrode after immobilization of antibody is a crucial factor which will confirm the decrease in current is only due to antibody-antigen interaction. The parameters like incubation time, methanol concentration have been optimized to achieve better sensitivity.

4.7.1.1 Electrochemical stability of the BSA/anti-AFB_1/AuNPs/PEDOT/GCE bioelectrode:

The stability of the synthesized electrode was investigated by taking cyclic voltammetry at 20mV/s vs. Ag/Ag/Cl for 50 consecutive cycles in 100mM PBS and 5mM $[Fe(CN)_6]^{3-/4-}$ and it is shown in Figure 4.11. It is observed that there is no decrease in peak current intensity and the area of CV remains constant. It implies that there is no degradation in the electrode and its performance towards redox probe

$Fe[(CN)_6]^{3-/4-}$. It is known that the charge storage capacity of a modified electrode is proportional to the covered area of the CV curve, and therefore it is used as a parameter to estimate the stability of the BSA/anti-AFB1/AuNPs/PEDOT/GCE. Positively, as shown in Figure 4.9 the charge storage capacity of BSA/anti-AFB1/AuNPs/PEDOT/GCE retained 98.7% of initial value after 50 cycles, indicating high stability of the BSA/anti-AFB1/AuNPs/PEDOT/GCE composite.

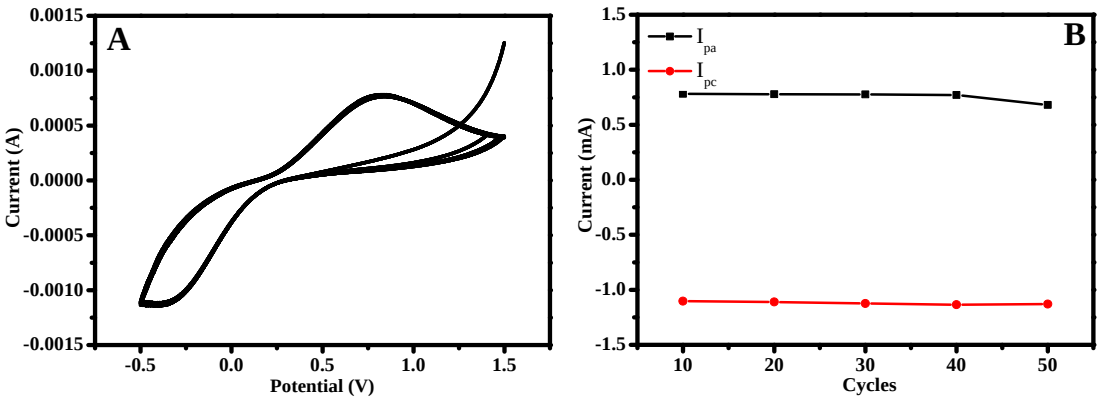

Figure 4.11: (A) Cyclic voltammogram of BSA/anti-AFB_1/AuNPs/PEDOT/GCE in 100mM PBS and 5mM $Fe[(CN)_6]^{3-/4-}$ and (B) The variation of I_{pa} and I_{pc} with respect to the number of cycles.

4.7.1.2 Determination of Optimized conditions for immunoassay of AFB_1:

In order to optimize the immunoassay conditions, the effects of the incubation time and methanol concentration were investigated. The toxin AFB_1 is completely insoluble in nonpolar solvents whereas it is soluble in slightly polar solvents like methanol and acetonitrile [295]. The presence of organic solvent during immunoreaction may result in antibodies denaturation as they are very susceptible to these solvents [367] Therefore the study of the effect of methanol concentration on the antigen antibody interaction was also performed. AFB_1 stock solutions were prepared with 30 ng/mL AFB_1 and different methanol concentration. Figure 4.12 shows the DPV peak current change ($\Delta I = I_0 - I_i$) increase up to 35% of methanol concentration and decreases sharply with further increase in concentration of methanol. It has been reported [368] that the AFB_1 conjugated with anti-AFB_1 is

partially redissolved in methanol on the surface of the electrode which can be decremented from the antibodies binding site as the concentration of methanol exceeds 50%. The lower concentration of methanol (10%) was optimized for further experiments to remove any unfavourable condition during the immunoreactions.

The incubation time of antigen and antibody interaction is another important parameter to be optimized. Figure 4.13 (A) is the DPV pattern of BSA/anti-AFB_1/AuNPs/PEDOT/GCE in 100mM PBS and 5mM $Fe(CN)_6^{3-/4-}$ (Blank) and 100mM PBS and 5mM $Fe(CN)_6^{3-/4-}$ with addition of 30 ng/ml of AFB_1 at an interval of 6 min, 12 min and 18 min respectively. As shown in Figure 4.13 (B) the DPV peak current change ΔI (I_0-I_i) increases gradually until 6min. Thus 6 min was chosen as the optimized incubation time required for antigen and antibody interaction in the successive experiments. All the experiments were performed at room temperature for enhanced practical application of the fabricated immunosensor.

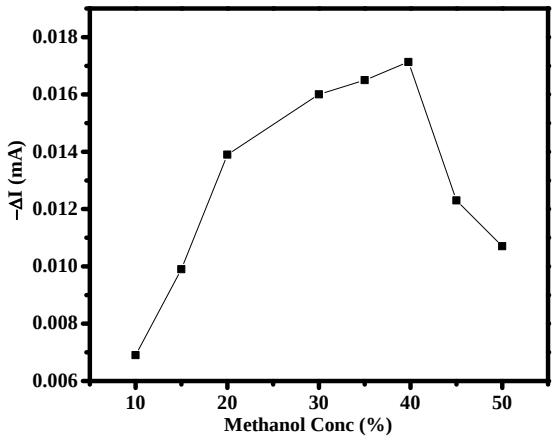

Figure 4.12: The variation of ΔI of BSA/anti-AFB_1/AuNPs/PEDOT/GCE in 100mM PBS and 5mM $Fe[(CN)_6]^{3-/4-}$ containing 30 ng/mL AFB_1 with different methanol concentration.

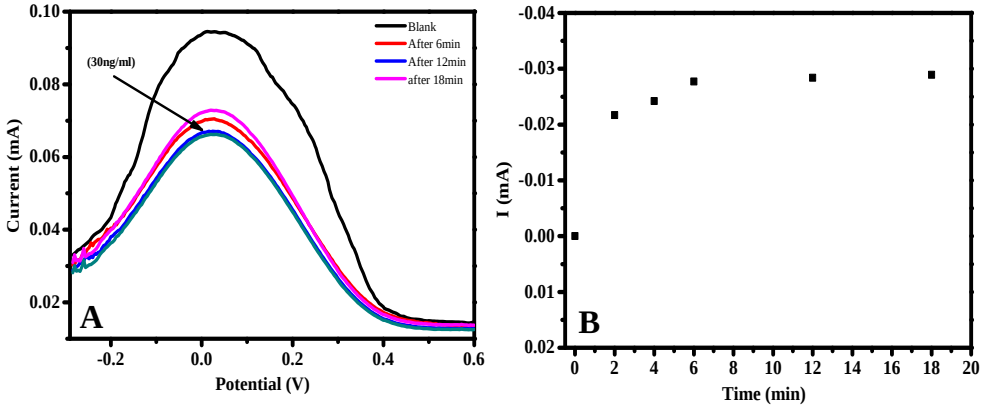

Figure 4.13: The DPV pattern of BSA/anti-AFB_1/AuNPs/PEDOT/GCE containing 30 ng/mL of AFB_1 in 100mM PBS and 5mM $Fe[(CN)_6]^{3-/4-}$ at an interval of 6 min, 12 min and 18 min.

4.7.2 Analytical Performance of the Immuno-electrode BSA/anti-AFB_1/AuNPs/GCE:

The response of the synthesized immunosensor BSA/anti-AFB_1/AuNPs/GCE towards its analyte AFB_1 was performed in 100mM PBS and $Fe[(CN)_6]^{3-/4-}$ with varying concentration of AFB_1 from 1ng/mL to 60 ng/ml and recorded using DPV as shown in Figure 4.14 (A). The peak current was found to be inversely proportional to the concentration of AFB_1. It has been reported [352] that the formation of antigen and antibody complex onto the immunoelectrode hinders the transfer of electron from redox probe $Fe[(CN)_6]^{3-/4-}$ to the electrode. The calibration curve in Figure 4.14 (B) shows a linear increase in the value of ΔI at lower concentration and gradually a steady state has reached where no further increase in current was observed.

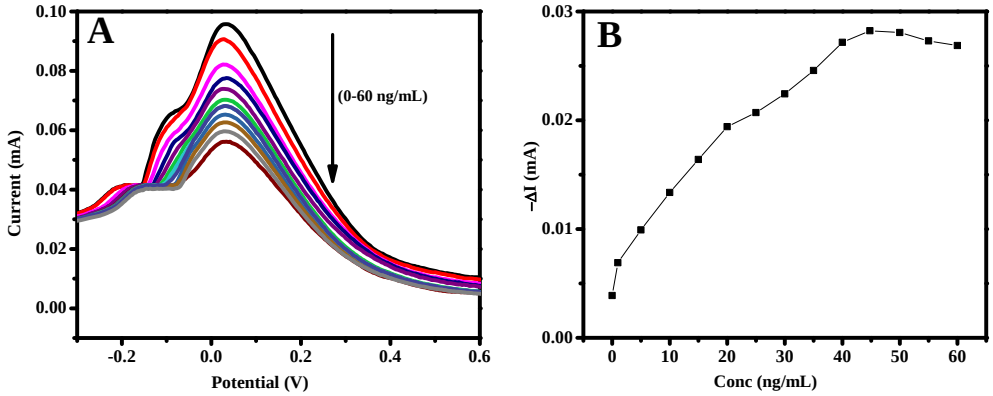

Figure 4.14: (A) The DPV pattern of BSA/anti-AFB_1/AuNPs/PEDOT/GCE with different concentration of AFB1 (1-60 ng/mL) in 100mM PBS and 5mM $Fe[(CN)_6]^{3-/4-}$ (B) The Calibration plot of change in current (ΔI) vs. Concentration in ng/mL.

Linearity plot is shown in figure 4.15 and linear response is found in two range 0.1-20 ng/mL and 20-40 ng/mL with regression equation of linearity plot as follows:

$$y = 0.725\ \mu A n g^{-1} m L\ [x] + 0.00548\ ;\ R^2 = 0.97 \qquad 4.11$$

$$y = 0.431\ \mu A n g^{-1} m L\ [x] + 0.0097\ ;\ R^2 = 0.98 \qquad 4.12$$

Where y is the DPV peak current change (ΔI) in μA and x is AFB_1 concentration in ng/mL. This corresponds to the sensitivity 0.725 $\mu AngmL^{-1}$ within a linear range of 1-20 ng/mL and 0.431 $\mu AngmL^{-1}$ with linearity 20-40 ng/mL, respectively. The limit of detection (LOD) and the limit of quantification (LOQ) were calculated from the parameters obtained from the regression curve, using $LOD=3*S_y/s$ and $LOQ=10*S_y/s$, where 'S_y' is the standard deviation of the y-intercept and's' is the slope. The calculated value of corresponding LOD and LOQ for the fabricated immunosensor is 0.0307 ng/mL and 0.102 ng/mL. The analytical parameters of the immunosensor BSA/anti-AFB1/AuNPs/GCE have been summarized in Table 4.7.

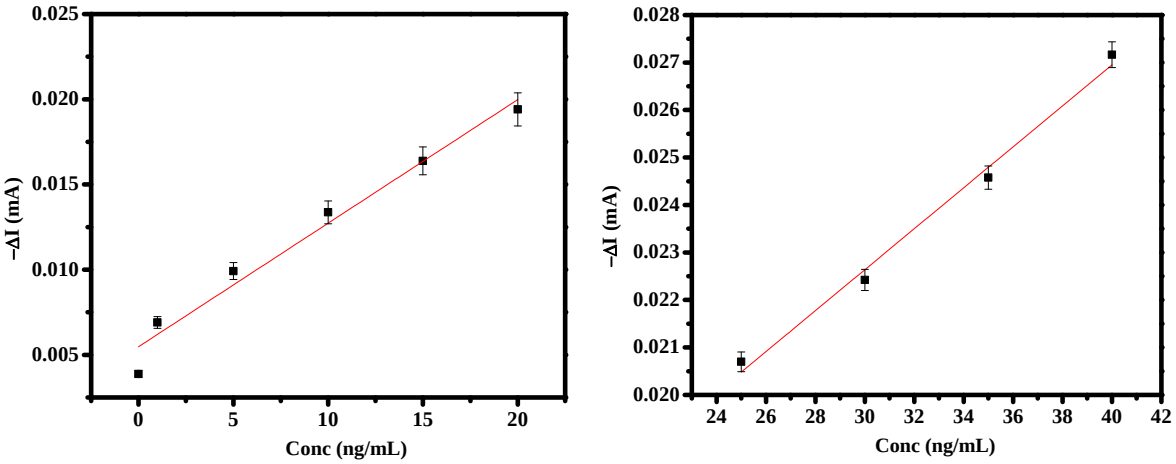

Figure 4.15: The linearity plot of BSA/anti-AFB_1/AuNPs/PEDOT/GCE towards the detection of AFB_1.

Table 4.7: Analytical Parameters of BSA/anti-AFB_1/AuNPs/PEDOT/GCE towards the detection of AFB_1.

Parameters	Values
Linearity range (ng/mL)	0.1-20 ng/mL; 20-40 ng/mL
Sensitivity	0.725 μAng^{-1}mL; 0.431 μAng^{-1}mL
Correlation Coefficient (R^2)	0.97, 0.98
LOD	0.0308 ng/mL
LOQ	0.102 ng/mL

4.7.3 Performance of the Immunosensor towards real sample:

The applicability of the synthesized bioelectrode BSA/anti-AFB_1/AuNPs/PEDOT/GCE has been studied in spiked real maize sample. DPV of BSA/anti-AFB_1/AuNPs/PEDOT/GCE in 100mM PBS and 5mM $Fe[(CN)_6]^{3-/4-}$ were recorded for real maize sample spiked with 20 ng/mL and 40 ng/mL AFB_1 and are shown in Figure 4.16 (A & B). The recovery experiments were performed using standard addition method and obtained results are presented in Table 4.8 and 4.9 and the recovery (%) has been calculated using:

$$Recovery\ Percentage\ (\%) = \frac{Measured\ value}{Expected\ value} \times 100 \qquad 4.13$$

It has been found the recovery (%) of the BSA/anti-AFB_1/AuNPs/PEDOT/GCE towards maize sample spiked with 20 ng/mL and 40 ng/mL AFB_1 are 94.89 % and 98.15 %respectively.

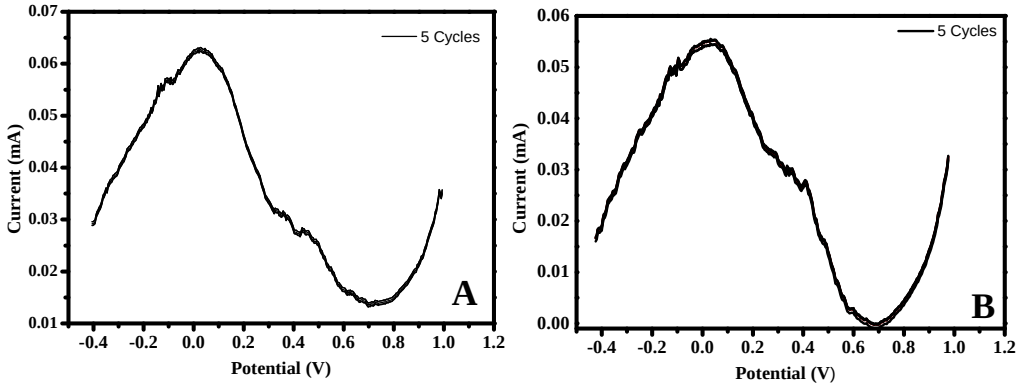

Figure 4.16: The DPV variation of peak current of BSA/anti-AFB1/AuNPs/PEDOT/GCE in 100mM PBS and 5mM $Fe[(CN)_6]^{3-/4-}$ containing real maize sample spiked with (A) 20 ng/mL and (B) 40 ng/mL respectively.

Table 4.8: Statistics and performance characteristics of the Working electrodes towards standard AFB_1 sample

Concentration of Aflatoxin	Measured Current (mA)	Average (x)	SD	RSD(%)
20 ng/ml	0.065	0.0654	0.001517	0.441842
	0.068			
	0.064			
	0.065			
	0.065			
40 ng/ml	0.054	0.0552	0.001306	0.789639
	0.057			
	0.054			
	0.055			
	0.056			

Table 4.9: Statistics and performance characteristics of the Working electrodes towards standard AFB_1 sample spike with maize.

Concentration of Aflatoxin Spiked (Conc of spiked/ standard AFB_1) (1:3)	Measured Current (mA)	Average (x)	SD	RSD (%)
20 ng/ml	0.063	0.062	0.00071	0.804123
	0.062			
	0.062			
	0.061			
	0.062			
40 ng/ml	0.055			
	0.054			
	0.054			
	0.052			
	0.055	0.054	0.001224	2.26

4.8 Application of AChE/AuNPs/PEDOT/GCE to detect Organophosphate (methyl parathion):

Acetylcholine esterase (AChE) based biosensor for the detection of pesticides is based on the principle of monitoring the decrease in enzymatic activity of AChE towards its analyte 'Acetylthiocholine Chloride (AThCl)' in presence of pesticides [334].

4.8.1 Analytical behavior of AChE/AuNPs/PEDOT/GCE towards Acetylthiocholine Chloride (AThCl):

The enzymatic behaviour of AChE immobilized on the matrix of AuNPs/PEDOT/GCE towards its analyte acetylthiocholine chloride (AThCl) has been studied using cyclic voltammetry. Figure 4.17 shows the cyclic voltammogram pattern of AChE/AuNPs/PEDOT/GCE in absence and in presence of different concentration of AThCl. In absence of AThCl no visible peak current is observed which indicates no redox activity of AChE in PBS. In presence of AThCl (1mM), an oxidation peak at 0. 82 V was observed which is may be due to oxidation of

thiocholine (RSH) (equation 4.14) [369]. The oxidation peak current increases with increasing concentration of AThCl which implies increasing oxidation of thiocholine in presence of enzyme. The generic reaction in presence of AChE can be described by the following equations [369]:

$$Acetylthiocholine\ chloride \xrightarrow{AChE} thiocholine + acetic\ acid$$

$$Thiocholine\ (red) \rightarrow disulfide\ (Ox) + 2H^+ + 2e^- \qquad 4.14$$

The effect of scan rate on the catalytic behaviour of the enzyme electrode towards its analyte has been studied and it is displayed in Figure 4.18 (A). The linear variation of the anodic current with scan rate (Figure 4.18 (B)) indicates the diffusion controlled process. The effect of increasing concentration of AThCl on the activity of the AChE entrapped in AuNPs/PEDOT/GCE has been further studied using differential pulse voltammetry. Figure 4.19 (A) shows the DPV pattern of AChE/AuNPs/PEDOT/GCE in 100 mM PBS in absence of AThCl (blank) and with increasing concentration of AThCl ranging from 0.1 mM to 7 mM. The intensity of current was found to be increasing initially and saturation occurs as we go on increasing the concentration of AThCl.

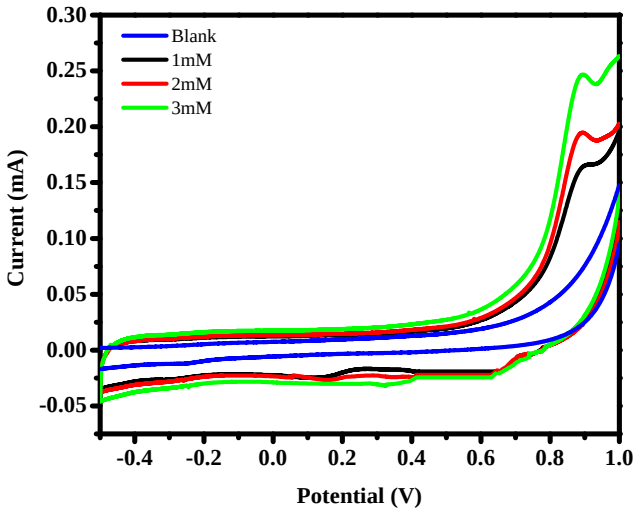

Figure 4.17: The cyclic voltammogram of AChE/AuNPs/PEDOT/GCE in 100 mM PBS in absence and presence of different concentration of AThCl at a scan rate of 5 mV/s vs. Ag/AgCl.

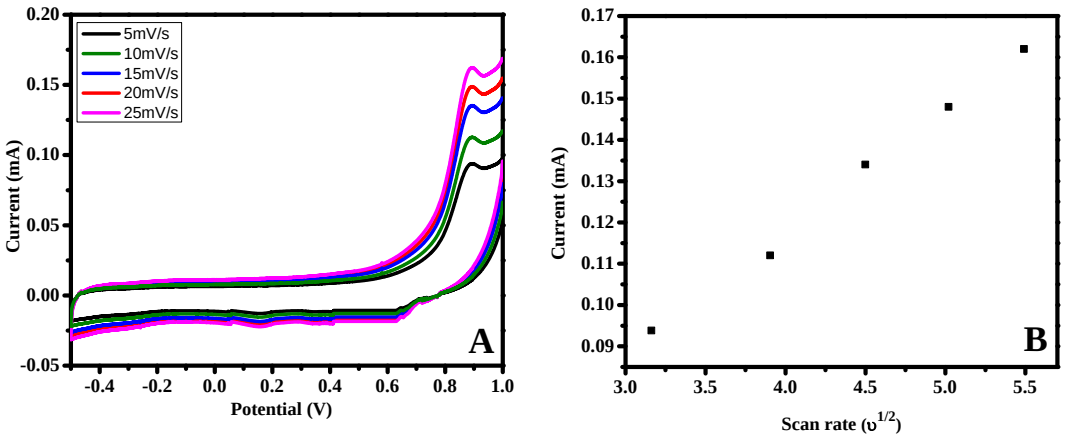

Figure 4.18: The cyclic voltammogram of AChE/AuNPs/PEDOT/GCE in 100 mM PBS and 2 mM AThCl in different scan rate and (B) Linear variation of peak current (I_{pa}) vs. square root of scan rate ($\upsilon^{1/2}$).

The variation of peak current versus the concentration follows Michaelis Menten pattern as it increases with increasing concentration of AThCl and saturation occurs. The value of Michaelis Menten constant 'K_m' has been calculated from lower linear part of calibration plot using equation 4.12 [266]:

$$\frac{1}{i} = \frac{1}{I_{max}} + \frac{K_m}{I_{max}[AThCl]} \qquad 4.15$$

Where I_{max} corresponds to the saturation current of thiocholine oxidation.

The value of K_m and I_{max} was found 0.823 mM and 171 μA, respectively.

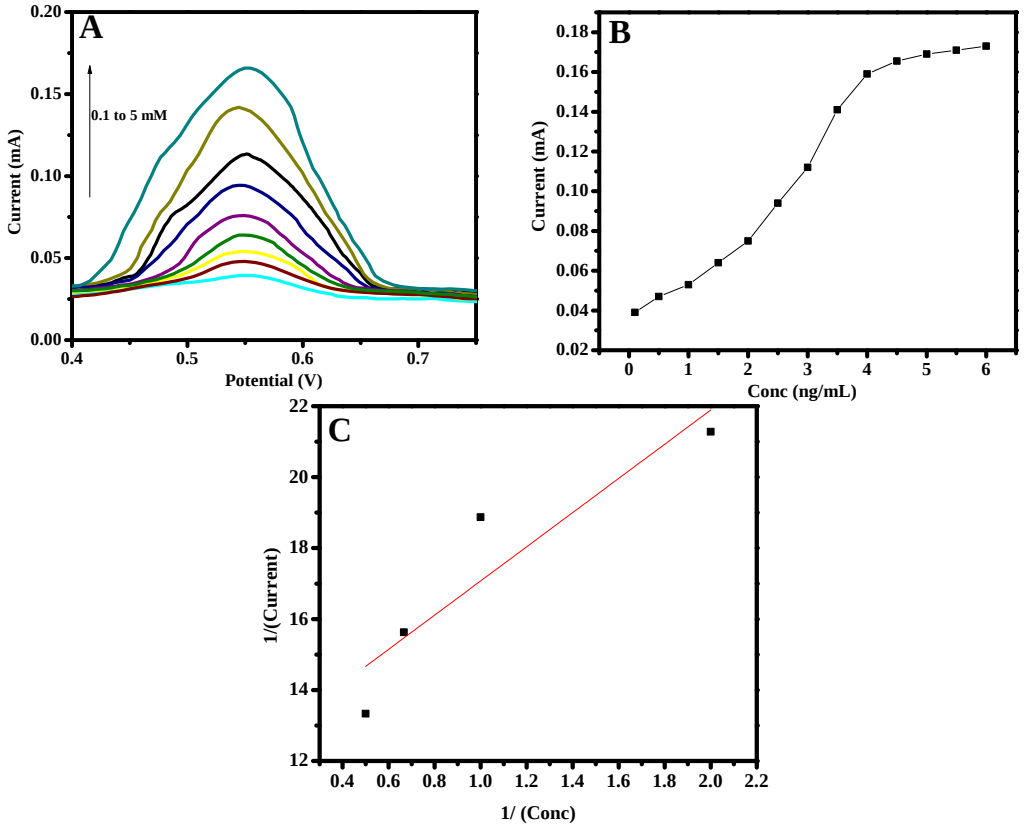

Figure 4.19: The DPV pattern of AChE/AuNPs/PEDOT/GCE in 100 mM PBS and in presence of different concentration of AThCl , (B) calibration plot of peak current vs. concentration of AThCl in ng/mL and (C) Lineweaver Burk plot of reciprocal of current and concentration.

4.8.2 The effect of pH on electro-catalytic behaviour of AChE/AuNPs/PEDOT/GCE:

The cyclic voltammetry of the AChE/AuNPs/PEDOT/GCE in presence of 2 mM AThCl in 100 mM PBS of different pH ranging from 6.5 to 8. The oxidation potential shifts towards lower potential side with the increasing pH. The Pourbaix diagram (E_{pa} vs. pH) is displayed in Fig (4(C & D)) and the pH dependence of the oxidation peak potential shows a linear variation with regression equation $E_{pa} = 0.062\,pH + 1.34$ with a slope of 62 mV/pH. This value is close to the theoretical value of 59 mV/pH calculated according to the Nernst equation, this behaviour indicates equal number of electron and proton transfer reaction [251].

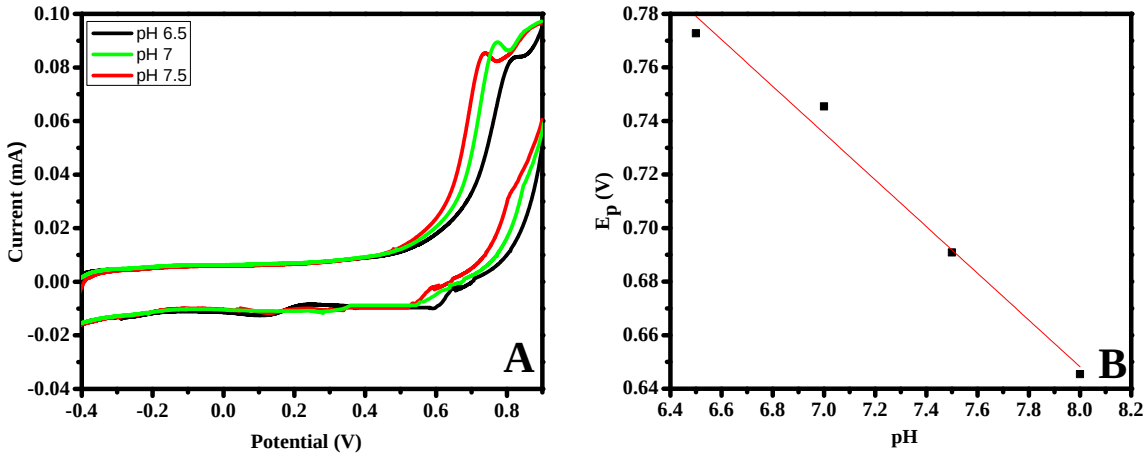

Figure 4.20: The CV of AChE/AuNPs/PEDOT/GCE in 2 mM AThCl and 100 mM PBS of different pH ranging 6.5 to 8 and (B) Plot of variation of the peak potential with pH of the solution.

4.8.3 Optimization of experimental parameters:

The experimental parameters like enzyme loading and incubation time have been optimized. The enzyme loading is another crucial factor to be optimized and it has been found that the amperometric response increases up to 5 µL of 50 U (stock) solutions. Further increase in the enzyme loading decreases the signal from substrate which is due to the limited electrode area where large volume of enzyme loading is unstable. Therefore, a volume of 5 µL of AChE was chosen as the optimal volume for preparation of the biosensor.

Incubation time is an important parameter in AChE inhibition based biosensor, which depends on the pesticide toxicity and dosage [370]. The inhibition effect on AChE activity at different incubation times 2 min-10 min was studied in 10 ng/mL methyl parathion. The dependence of incubation time on inhibition ratio shows saturation and loss of enzyme activity when incubated for a longer period of more than 8 min Figure 4.21 (A & B). Therefore the optimized incubation time of 6 min was fixed for the further experiments to get better sensitive pesticide biosensor.

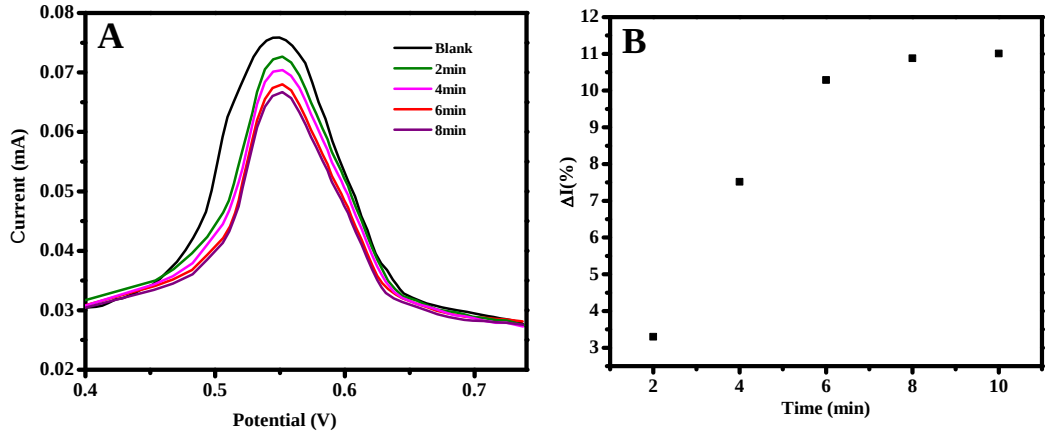

Figure 4.21: The DPV of AChE/AuNPs/PEDOT/GCE in 2 mM AThCl and 100 mM PBS in presence of 10 ng/mL MP after different incubation time and (B) Plot of variation of the I(%) with time in min.

4.8.4 Inhibition Studies towards the pesticides samples:

At the optimum fabrication conditions, the analytical performance of the synthesized enzyme electrode towards methy parathion (MP) was evaluated. The detection method is based on measuring the DPV current in 2mM AThCl before (curve a) and after (curve b) incubation with different concentration of pesticides. I_{cat} value decreased from 0.075 mA (blank) to 0.039 mA (55 ng/mL) due to the inhibition methyl parathion, respectively.

The percentage of Inhibition (I %) and residual enzyme activities were calculated using equations (1) & (2) [371] :

$$Inhibition\ \%\ (I\%) = [(\frac{I_0 - I_i}{I_0}) \times 100] \quad (4.16)$$

$$Residual\ enzyme\ activity\ \%\ (REA\ \%) = \left[\frac{I_i}{I_0}\right] \times 100 \quad (4.17)$$

where I_i and I_0 is the measured DPV current in 2 mM AThCl and 100 mM PBS in absence and in presence of pesticide.

In presence of MP, the activity of immobilized AChE decreases as the enzyme-inhibitor complex blocks the active site of the enzyme [372]. It results in less or no production of thiocholine and hence decreased in the oxidation current occurs according to equation 4.14. The plot of inhibition I% vs. concentration of MP shows

an increase in the inhibition of enzyme activity with increasing concentration and finally saturation occurs.

The AChE/AuNPs/PEDOT/GCE shows linearity in the range 0.1 ng/mL-35 ng/mL with regression equation of

$$I(\%) = 1.07\,[AThCl] + 0.050;\ R^2 = 0.99 \qquad 4.14$$

The results indicate that the bioelectrode AChE/AuNPs/PEDOT/GCE is an efficient sensor for the detection of the pesticide.

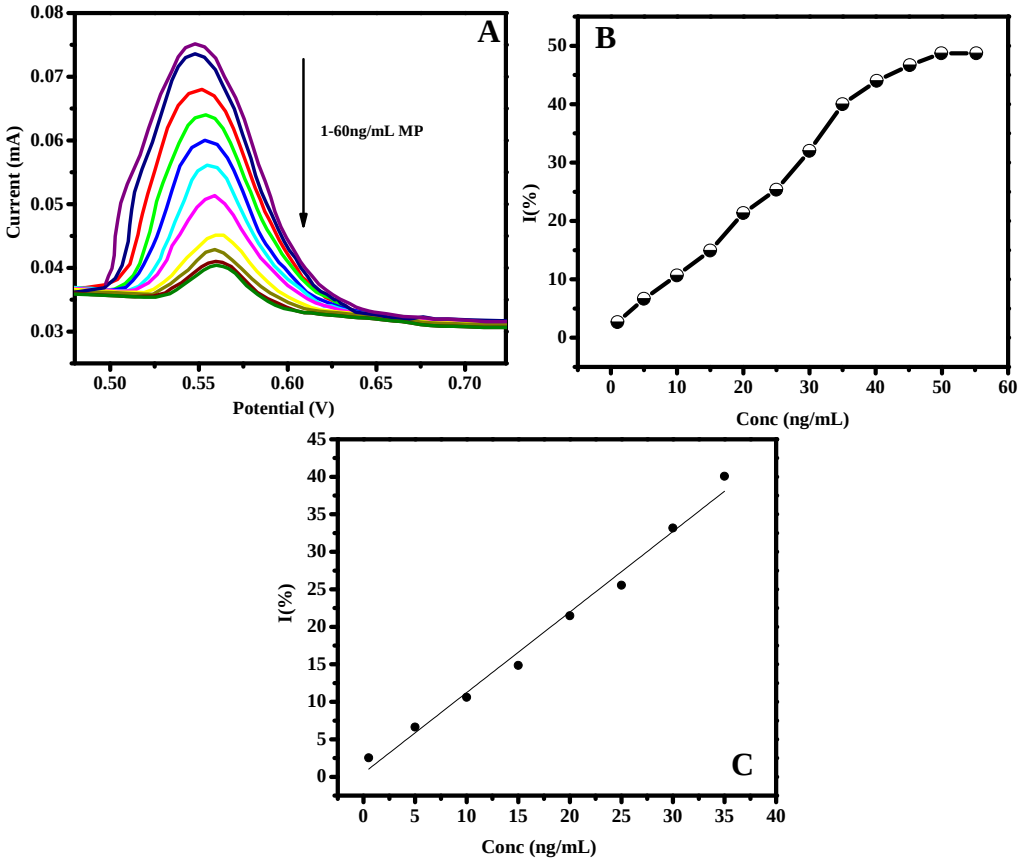

Figure 4.22: The DPV pattern of AChE/AuNPs/PEDOT/GCE in 100 mM PBS and 2 mM AThCl and different concentration 0.1 ng/mL to 55 ng/mL, B) Calibration of plot of I (%) versus concentration (C) Linear response towards MP inhibition.

Figure 4.24 shows the calibration plot of residual enzyme activity (%) vs. the concentration of the pesticides. After inhibition, the residual activity is the small fraction of the enzyme that remains active into the matrix of AuNPs/PEDOT/GCE and as the pesticides sample concentration increases the residual activity decreases with time. The immobilized enzyme retains 53% of its activity after the pesticides inhibition. The response is further studied by determining the limit of detection (LOD) and limit of quantification (LOQ) using the relation $3\times S_0/S$ and $10\times S_0/S$, where S_0 is the slope of the calibration plot taken for minimum concentration of the pesticides sample. The shelf life of the AChE/AuNPs/PEDOT/GCE electrode has been studied and found that the biosensor showed a good activity of recovery of 84% after weekly usage and 80 days storage in phosphate buffer at 5^0C.The analytical parameters towards the response of methyl parathion have been tabulated in Table 4.11.

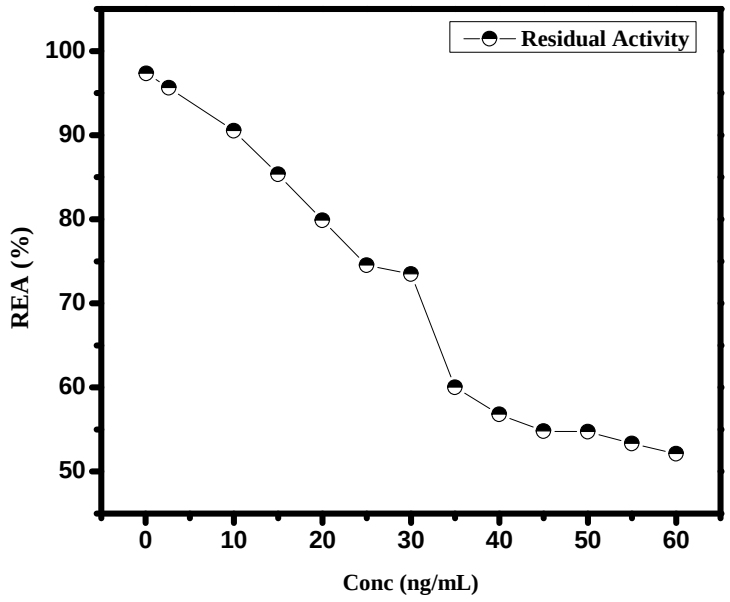

Figure 4.23: Residual enzyme activity percentage (REA %) of AChE after methyl parathion inhibition.

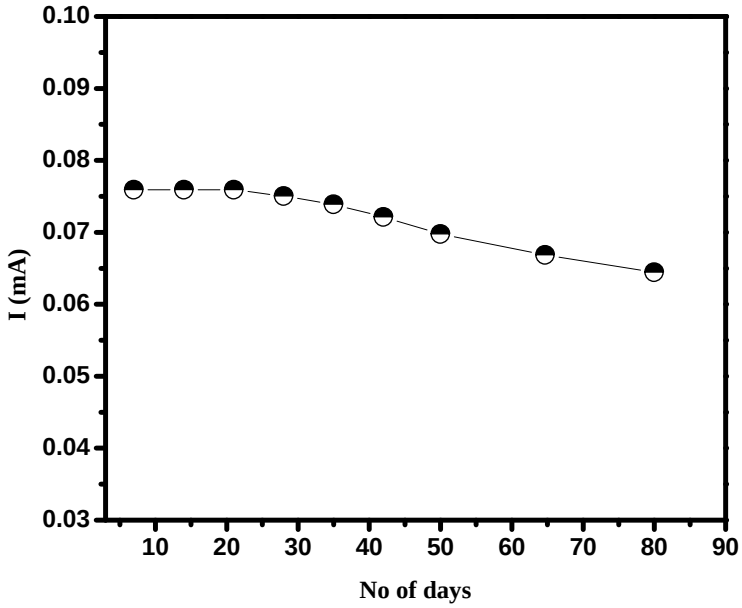

Figure 4.24: Shelf life study of the immobilized AChE and its activity of AThCl.

Table 4.10: Analytical parameters of AChE/AuNPs/PEDOT/GCE towards Methyl parathion inhibition.

Parameters	**Towards Methyl Parathion**
Linearity (ng/mL)	0.1 ng/mL- 35 ng/mL
Sensitivity	1.07 $(ng/mL)^{-1}$
Correlation Coefficient (R^2)	0.99
LOD	0.708 ng/mL
LOQ	2.36 ng/mL

4.9 Summary:

PEDOT and PEDOT functionalized with Au-NPs have been synthesized and their morphological and structural properties have been investigated. SEM micrograph confirms the uniform distribution of Au nanoparticles of average size 230 nm to 300 nm on the porous surface of PEDOT. The contact angle of water droplet on AuNPs modified surface is found to be 54^0 which depicts the hydrophillic nature of the film. The anti-AFB_1 and AChE have been immobilized using EDC/NHS coupling to synthesize BSA/anti-AFB_1/AuNPs/PEDOT/GCE and AChE/AuNPs/GCE. FTIR results show the characteristic bonding of different functional groups in PEDOT and the binding of anti-AFB_1 with the PEDOT/Au-NPs/GCE matrix. The cyclic voltammetry in redox active solution shows improved performance of AuNPs/PEDOT/GCE by decreasing the value of ΔE_p (176 mV) and enhancing the current values (I_{pa} and I_{pc}). The linear change in the intensity of I_{pa} and I_{pc} with the scan rate of application of voltage vs. Ag/AgCl suggests a diffusion controlled process. The slopes of the regression equation of the linear plot of current vs. scan rate have been used to calculate the electro active surface area. The three fold increase in the area of GCE after deposition of AuNPs over PEDOT composite film implies that nano gold provides a large surface area which is more suitable for the protein immobilization. Similarly the surface coverage of the ionic species (AChE and anti-AFB_1) is found to be 1.16×10^{-5} mol cm^{-2} and 6.7×10^{-6} mol cm^{-2}, respectively. AuNPs not only help in better immobilization but also improve the charge transfer within the matrix which is inferred from the decreased value of R_{et} (67Ω) and enhanced value of k_s (1.91×10^{-2} s^{-1}).

The immunoelectrode BSA/anti-AFB_1/AuNPs/PEDOT/GCE shows a stability of 98% over 50 consecutive cycles of cyclic voltammetry implies that there is no degradation in electro-active property of the electrode. The immunosensing in presence of different concentration of AFB_1 has been performed by keeping the electrode dipped in AFB_1 solution for 6 mins. The DPV peak current is inversely proportional to the concentration of antigen and as the formation of antigen-antibody complex onto the surface of the immunoelectrode hinders the transfer of electron between redox probe $Fe[(CN)_6]^{3-/4-}$ and the immunoelectrode. The sensitivity of the immunoelectrode BSA/anti-AFB_1/AuNPs/PEDOT/GCE has been determined to be

0.725 μAng-^{1}mL and 0.431 μAng-^{1}mL in two linear regions of 0.1 -20 ng/mL; 20 - 40 ng/mL of AFB_1 concentration, respectively.

The enzyme (AChE) immobilized electrode, AChE/AuNPs/PEDOT/GCE, showed an oxidation peak in cyclic voltammogram at around 0.82 V vs. Ag/AgCl corresponding to oxidation of thiocholine. Therefore AuNPs/PEDOT/GCE can be considered as biocompatible electrode which provides ideal environment to keep the activity of immobilized AChE. The enzyme kinetics was studied using DPV by monitoring the oxidation peak current with increasing substrate concentration form 0.1 mM to 5 mM. The K_m and I_{max} of AChE/AuNPs/PEDOT/GCE towards the hydrolysis of acetylthiocholine is found to be 0.823 mM and 171 μA. Small value of K_m depicts good enzymatic performance of AChE towards its analyte which represents an efficient transfer of electrons between the electrode surface and active site of AChE. In presence of methyl parathion the electrode showed a linearity of 0.1 to 35 ng/mL with sensitivity (I% per unit change in concentration) of 1.07 ng/mL with LOD and LOQ of 0.708 ng/mL and 2.36 ng/mL, respectively.